Research Article

Received: 14 December 2014 Revised: 8 February 2015 Accepted article published: 5 March 2015 Published online in Wiley Online Library: 25 March 2015

(wileyonlinelibrary.com) DOI 10.1002/pi.4909

Effect of morphology on the permeability, mechanical and thermal properties of polypropylene/SiO_2 nanocomposites

Moisés Gómez,* Diego Bracho, Humberto Palza and Raúl Quijada

Abstract

Spherical silica nanoparticles with 20 and 100 nm diameters and organic-template layered silica nanoparticles synthesized by the sol-gel method were melt blended with a polypropylene (PP) matrix in order to study and quantify their effect on the oxygen and water vapor permeability and mechanical and thermal behavior. With regard to barrier properties, the spherical nanoparticles barely increased the oxygen permeability at low loads (≤10 wt%); meanwhile the layered nanoparticles dramatically increased it even at low loading (<5 wt%) probably due to the percolation effect. The changes in water vapor permeability were similar to those in oxygen permeability. The repulsive interaction between nanoparticles and PP forms interconnecting voids where the gas permeates. Tensile stress–strain tests showed that the composites present up to a 56% increase in the elastic modulus with spherical nanoparticles at 20 wt%, while layered nanoparticles show a decrease probably due to agglomerations and voids. Thermogravimetric analysis under inert conditions showed that the nanoparticles improved the PP thermal degradation process through the adsorption of volatile compounds on their surface, where the smaller spherical nanoparticles show the greatest stabilization.

Keywords: polypropylene nanocomposites; silica nanoparticles; permeability; mechanical properties; thermal properties

INTRODUCTION

The development of polymer-based nanocomposites has grown into a wide and promising area in research from both academic and industrial standpoints. A polymer nanocomposite is a multiphase material consisting of a continuous polymeric phase and a dispersed phase of nanometric dimensions.[1–6] The great interest in these materials is based on the possibility of greatly enhancing the properties of a given matrix by adding small amounts of nanometric fillers (<10 wt%), compared to the traditional microcomposite loads (<30 wt%). Due to the high specific surface area of the nano-sized particles, it is possible to obtain the same or better property enhancement by using smaller loads than with traditional microfillers.[6]

Polyolefins such as polypropylene (PP) are of particular interest as polymer matrices due to their low production cost, facile processability and good properties, especially for industrial applications.[4,7,8] On the other hand, natural aluminosilicate clays have been widely studied over the past two decades as inorganic fillers in polymer composites.[3] These clays are usually chemically modified in order to exfoliate their lamellar structure prior to the composite blending.[3,9] The low cost and easy access to these natural clays is one of their great advantages; however, geometry and size are restricted by their natural occurrence and are key variables in the study and development of polymer nanocomposites.[10,11] In addition, natural impurities remain in the clays, affecting properties of the nanocomposites such as color, magnetic properties, optical properties etc.[11] For these reasons, a novel route is to use synthetic nanoparticles as fillers, produced by the sol-gel process, which yields products with high composition homogeneity, purity and reproducibility.[12] Additionally, this method can be adapted in order to produce nanoparticles in a wide range of sizes and geometries, including spheres[13] and sheets.[11] Two of the major advantages of the method are the mild reaction conditions, such as relatively low temperature and pressure, and the synthesis of highly pure materials.[6,12,14]

Gas transport in nonporous polymer membranes typically proceeds by a solution-diffusion mechanism in which the permeability (P) can be calculated using $P = SD$,[6] where S and D denote the solubility and diffusivity of the permeating species, respectively. It is well known that the presence of nonporous particles, such as silica nanoparticles, in conventional filled polymer (PP, polyethylene etc.) systems typically reduces the permeability of the polymer. The filler reduces the free volume available for gas sorption within the polymer, reducing the solubility factor and the diffusivity by a tortuous path mechanism.[3,6,15] However, in 2002 Merkel *et al.*[16] discovered that the addition of nanometer-sized silica particles in polymers could systematically increase the gas permeability due to an increase of the polymer free volume at the polymer – particle interface, caused by a weak interaction between particles and polymer.[6,17] Dougnac *et al.* reported that the addition of spherical nanoparticles with different diameters synthesized by the sol-gel method in PP increases O_2 and N_2 permeability.[18]

* *Correspondence to: Moisés Gómez, Departamento de Ingeniería Química y Biotecnología, FCFM Universidad de Chile, Beauchef 850, Santiago, Chile. E-mail: mogomez@ing.uchile.cl*

Departamento de Ingeniería Química y Biotecnología, FCFM Universidad de Chile, Beauchef 850, Santiago, Chile

Others authors have found a decrease of the permeability to O_2, N_2, CO_2 and other gases in different polymer (PP, polyethylene etc.) nanocomposites.[9,19,20]

One of the primary reasons for adding inorganic fillers to polymers is to improve their mechanical performance whilst balancing strength, stiffness and toughness.[1,4,6] It has often been found that the mechanical properties of nanocomposites are strongly dependent on filler content. In PP composites with 10 wt% silica nanospheres of 20 and 100 nm diameter an increase in Young's modulus of 40% and 18%, respectively, was found.[21] In PP composites with layered silica nanoparticles, an increase in the elastic modulus of 8% has been reported at 1 wt%, decreasing linearly at higher loadings (≥3 wt%), due to a weak interaction between the polymer and the nanoparticles.[14] For thermal properties, on the other hand, the incorporation of nanometer-sized inorganic particles into the polymer matrix typically enhances the thermal stability by acting as a superior insulator and mass transport barrier to the volatile products generated during decomposition.[6,14] Moncada *et al.* reported that the addition of spherical and layered silica nanoparticles synthesized by the sol-gel method increases the thermal stability of PP under oxidative conditions.[22] Furthermore, it has been found that the addition of spherical nanoparticles of *ca* 70 nm can dramatically improve the thermal degradation of PP.[2] The enhancement of the mechanical and thermal properties in polymer nanocomposites can be attributed to the high rigidity of the nanoparticles along with the high interfacial interaction between the polymer matrix and the surface of the dispersed nanoparticles.[2,4,6,14,21]

Based on this, the permeability and mechanical and thermal properties of the polymer matrices can be tailored by adding different nanofillers, although the global effect is not yet fully understood.[14] In this work, PP nanocomposites were prepared using spherical and layered silica nanoparticles (SiO_2) synthesized by the sol-gel method in order to contribute to the understanding of the effect of their size and shape on the oxygen and water vapor permeability, mechanical properties and thermal stability.

EXPERIMENTAL

Materials

Tetraethoxysilane (≥98%, TEOS) and hexadecyltrimethoxysilane (≥85%, HDTMOS) were obtained from Sigma-Aldrich (St. Louis, MO, USA), and used as received. Ammonia (25 wt%) and hydrochloric acid (32 wt%) were obtained from Equilab (Santiago, Chile). Commercial isotactic PP (PP-H401) with a melt flow index of 7.5 g (10 min)$^{-1}$ and a density of 0.905 g cm^{-3} was obtained from Braskem (São Paulo, Brazil) and used as received. The antioxidant used in the preparation was a 2:1 mixture of Irganox 1010 and Irgafos 168.

Synthesis of spherical and layered SiO_2 nanoparticles

Silica nanospheres of 20 and 100 nm diameter were produced using a sol-gel method presented by our group in a previous work.[21] For layered silica nanoparticles, a sol-gel synthesis method was used based on the work of Chastek *et al*.[11]

Characterization

Elemental analyses for carbon and hydrogen were performed on a Leeman Labs Inc. CE440 elemental analyzer and a Control Equipment Corporation 440 elemental analyzer. Powder XRD patterns were recorded using a Siemens D-5000 wide-angle XRD spectrometer with Cu Kα radiation, operating at 40 kV and 45 mA. TGA was performed in an inert atmosphere (nitrogen) using an SDT (TGA-DSC) Q600 thermal analyzer. The samples were heated from 25 to 700 °C at a heating rate of 20 °C min^{-1}. Transmission electron microscopy (TEM) images were recorded digitally using a Philips Tecnai 12 microscope operating at 80 kV.

Nanocomposite blending

The PP/SiO_2 composites were produced by melt-mixing in a Brabender Plasti-Corder at 190 °C and 110 rpm for 10 min. Approximately 35 g per mixing was produced, containing PP, SiO_2 nanoparticles and a small spoonful of Irganox 1010:Irgafos 168 (2:1) antioxidants.

Testing of mechanical properties

Mechanical properties were measured using an HP D500 dynamometer with a strain rate of 50 mm min^{-1} at room temperature, according to ATSM D638.[23] Young's modulus was calculated as the slope of the linear elastic zone in the stress – strain curve.

Oxygen and water vapor permeability

The oxygen permeability test was performed using the time-lag method in a permeability cell built in our laboratory, whose design is described elsewhere.[18,24] The system was sealed hermetically and exposed to vacuum (10^{-3} bar) for 3 h before every test. The oxygen pressure was 2 bar for all the samples, and the temperature was kept constant at 30 °C. However, the water vapor permeability (WVP) was measured using the dry cup method.[25] The mass of the cups was measured every 24 h for 15 days.

RESULTS AND DISCUSSION

Synthesis of nanoparticles

TEM images of spherical and layered silica nanoparticles synthesized by the sol-gel method are shown in Fig 1. For spherical nanoparticles, the final size was controlled by changing the pH of the reaction medium, getting particles of approximately 20 and 100 nm in diameter (Fig. 1(a) and Fig. 1(b), respectively), denoted SNS20and SNS100, respectively. The exposed area per unit volume is inversely proportional to the particle diameter, and accordingly the SNS20 particles present high electrostatic forces generating greater agglomeration than the SNS100 particles,[26] as shown in Fig. 1(a).The presence of siloxane and hydroxyl groups, generated in the particle surface during the synthesis process, makes the silica surface highly hygroscopic, as previously reported.[6] Finally, Fig. 1(c) displays a typical TEM of silica layered nanoparticles, denoted SNL, showing cauliflower-like aggregation that avoids a proper characterization of the individual plates, as reported by other authors.[11,14] The dark zones correspond to agglomerations of the nanoparticles due to the attraction of the high organic content.[11] The layered geometry of the SNL was further confirmed by X-ray diffraction (Fig. 2). The interlaminar distance d_{001} (4.8 nm at 1.9°) indicates that the inorganic layers of SNL are separated by a bilayer arrangement of hexadecyl groups (C_{16}) as the corresponding 4.8 nm interlayer distance relates to approximately twice the length of the hexadecyl group, from the HDTMOS used in the synthesis.[11]

Table 1 shows the results of elemental analysis and the specific surface area of the silica nanoparticles. The inorganic content of the nanoparticles was obtained by TGA, based on the remaining mass after heating to 700 °C in inert conditions (N_2). The high carbon and hydrogen content in the SNL further confirmed the organic content. Moreover, the ratio between carbon

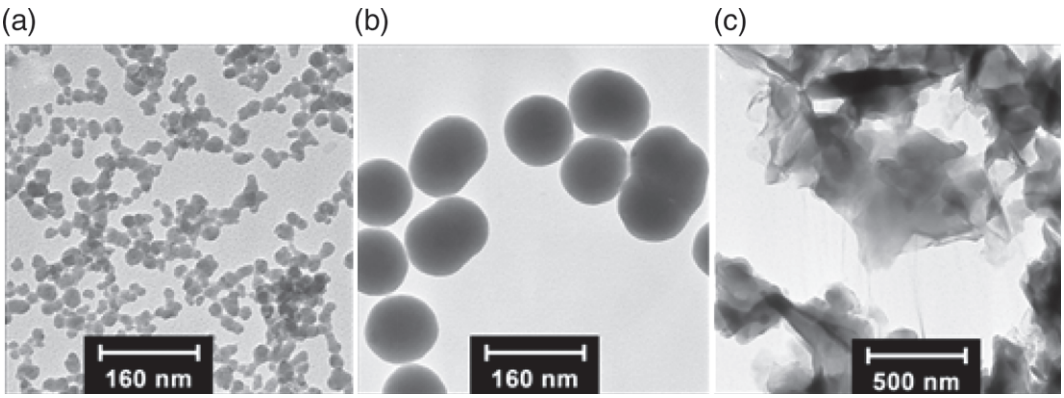

Figure 1. TEM images of the synthesized silica nanoparticles: (a) SNS20, (b) SNS100, (c) SNL.

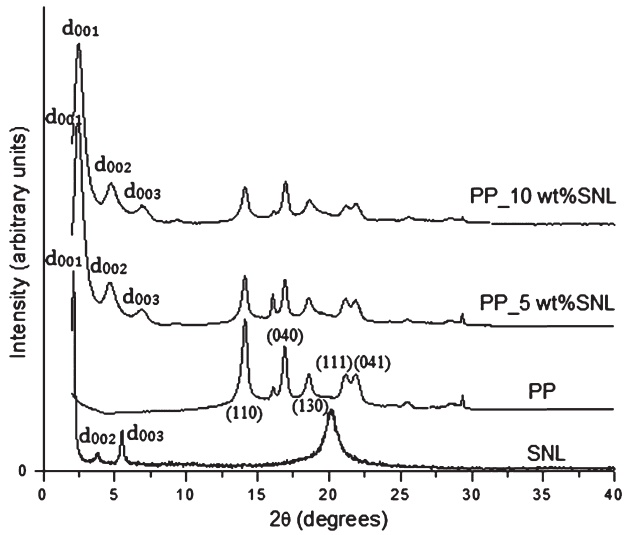

Figure 2. X-ray diffractograms of SNL nanoparticles and PP/SNL composites.

and hydrogen atoms in the hexadecyl groups (C_{16}) is *ca* 17/3, similar to the ratio obtained by elemental analysis (*ca* 16/3).

The spherical nanoparticles were calcined at 400 °C for 8 h to oxidize the unreacted TEOS, ethoxy groups and to evaporate the water absorbed on their surface before they were used in the composite preparation; thus the low carbon and hydrogen content is because these elements were not fully oxidized.[6,21] Furthermore, the agglomerates in the nanospheres shown in Fig. 1(a) and 1(b) could also be forming due to possible solid-state reactions that can occur during the calcination process, mainly condensation of silanol groups between particles, which can affect their morphological integrity.[21] On the other hand, the TGA of the SNL particles revealed two major events, gradual loss of water above 100 °C and degradation of the alkyl chains beginning at *ca* 180 °C, with major weight loss between 300 and 520 °C. For this reason, the SNL particles were dried at 100 °C before their incorporation. The low specific surface area of the SNL nanoparticles is due to the presence of hexadecyl groups on their surface, which confers their interlaminar distance.

Nanocomposites

Fig. 3 displays some representative TEM images from PP/SiO_2 composites with 10 wt% (inorganic content) of spherical (Fig. 3(a) and 3(b)) and layered (Fig. 3(c)) silica nanoparticles. For composites

Table 1. Elemental analysis and specific surface area for calcined SNS and dried SNL

	C (wt%)	H (wt%)	Inorganic content (wt%)	BET surface area ($m^2\ g^{-1}$)
SNS20	0.9	–	98.0	287.0 ± 0.7
SNS100	0.4	–	98.5	41.7 ± 0.2
SNL	63.6	12.0	23.5	8.1 ± 0.1

with spherical nanoparticles, agglomerated groups can be observed within the polymer matrix, with few individual particles. Because of the repulsive interaction between the hydrophilic silica surface and the hydrophobic PP matrix, as well as the high specific surface area, the SNS20 nanoparticles presented the largest agglomerations,[6,10] similar to those observed in pure particles (Fig. 1).The same behavior has been reported in similar PP/SiO_2 composite systems.[2,14] In the case of the layered nanoparticles, these are better dispersed in the polymer matrix, probably due to the presence of hydrophobic hexadecyl groups, increasing the affinity between the polymer and the nanoparticle surface. In addition, Fig. 3(c) shows either partially exfoliated particles or intercalated structures and some agglomerations (black areas). Based on these TEM images it can be estimated that the length of the layered nanoparticles has a value around 200 nm.

Fig. 2 also shows the XRD patterns for the PP/SNL composites which indicate a slight shift in the SNL interlaminar distances associated with higher angles (2.2°), reaching values of 4.1 nm (d_{001}). This can be explained by considering that some of the organic molecules can be expelled or start to degrade during the mixing process (190 °C),[27] where small molecules from the hexadecyl groups start to volatilize. This is consistent with the onset of SNL degradation (*ca* 180 °C). Furthermore, steric impediment when infiltrating layered structures with long polymer chains can generate a higher agglomeration degree, contributing to small crack formation in the polymer – particle interface.[10] On the other hand, the X-ray diffractograms show nearly the α-crystalline form of PP. In all cases, the monoclinic α reflections of PP can be found at 2θ angles of 14.2° (110 crystalline plane), 17.2° (040), 18.8° (130), 21.5° (111) and 21.9° (131 and 041). These observations confirm that the addition of SNL does not affect the crystalline polymorph of PP.[28]

Oxygen and water vapor permeability

The results for oxygen permeability and WVP are presented in Fig. 4. The SNL increased the oxygen permeability strongly

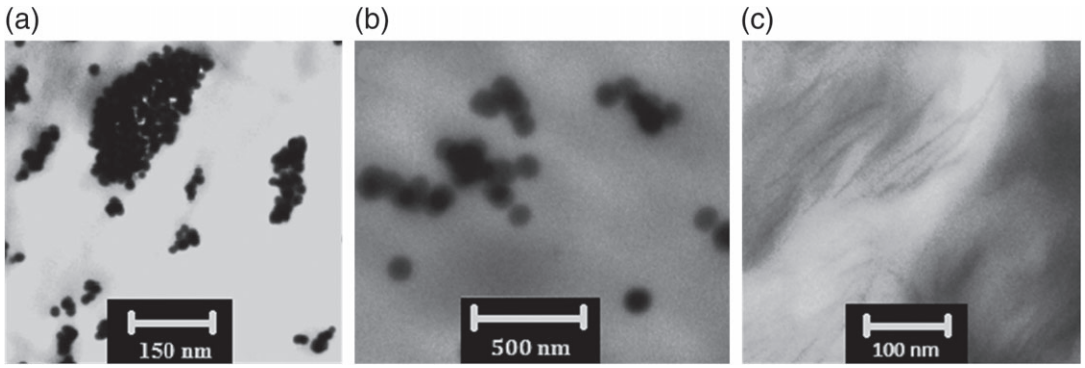

Figure 3. TEM images of PP/SiO_2 composites: (a) SNS20, (b) SNS100, (c) SNL.

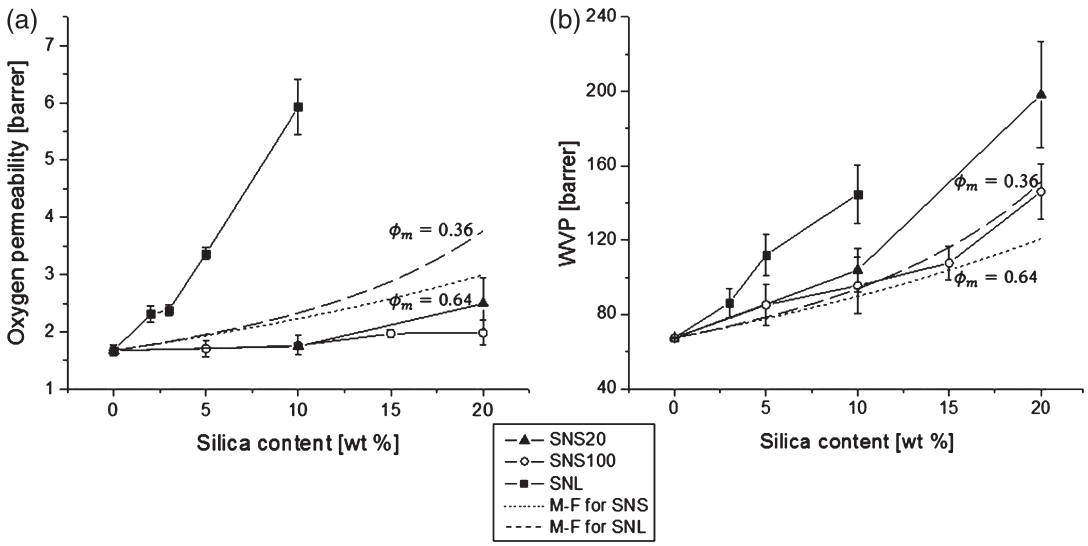

Figure 4. Permeability of the PP/SiO_2 composites: (a) oxygen permeability; (b) water vapor permeability (WVP).

(Fig. 4(a): at 2 wt% the permeability increased by 40%, while at 10 wt% it was increased by a factor of *ca* 3.5. On the other hand, the spherical nanoparticles have no significant effect at loadings of 5 – 10 wt%, and only at 20 wt% was there a significant increase of 20% and 50% in the oxygen permeability for SNS100 and SNS20, respectively. For a better understanding, the modified Felske (M-F) model was used, which estimates the composite permeability using the following equations:[29]

$$P_c = P_m \left[\frac{1 + 2\phi(\beta - \gamma)/(\beta + 2\gamma)}{1 - \psi\phi(\beta - \gamma)/(\beta + 2\gamma)} \right] \quad (1)$$

$$\psi = 1 + \left(\frac{1 - \phi_m}{\phi_m^2} \right) \phi \quad (2)$$

$$\beta = \left(2 + \delta^3\right)\left(P_p/P_m\right) - 2\left(1 - \delta^3\right)\left(P_i/P_m\right) \quad (3)$$

$$\gamma = 2 + \delta^3 - \left(1 - \delta^3\right)\left(P_p/P_i\right) \quad (4)$$

where P_m, P_p and P_i are the permeabilities of the polymer matrix (obtained experimentally), particles (considered impermeable) and voids (*ca* $100P_m$[29]), respectively; δ is the ratio of the outer radius of the interfacial shell to the core radius (1.45,[29] 'void size'); ϕ is the volume fraction of particles; and ϕ_m is the maximum value of ϕ, which is usually considered to be 0.64 and 0.36 for spheres and layered nanoparticles,[29] respectively. The M-F model predicts an increase of the permeability due to void formation in the polymer – particle interface by a weak interaction. In the case of the spherical nanoparticles ($\phi_m = 0.64$), the M-F model overestimates the results probably because it assumes a good dispersion of the filler material, which was not possible in this case (Fig. 3). On the other hand, the voids created by the agglomerations can overlap with each other, forming preferential permeation channels, which could even go across the entire polymeric film, an effect known as percolation.[30] However, the increase is probably lower because the void size is less than the assumed size (1.45); therefore the voids should be less than 9 and 45 nm for SNS20 and SNS100, respectively. The SNS20 nanoparticles cause greater changes than the SNS100 nanoparticles due to their higher specific surface area (Table 1) and agglomerate formation (Fig. 3), generating higher interfacial void volume. It is noted that no significant effect at low loadings is expected due to the low solubility between the oxygen (a polar molecule) and the polar silica surface. At higher loads, diffusion has more relevance than solubility due to the formation of preferential channels and voids in the composite.[6]

In the case of the SNL, the M-F model ($\phi_m = 0.36$) significantly underestimates the experimental results, probably due to their geometry and high aspect ratio favoring void interconnection.[6,17] It seems that the SNL allow the formation of a void percolation process increasing the permeability in a nonlinear way (shown in Fig. 4). In general, layered nanoparticles present

geometrical percolation at lower concentrations than spherical nanoparticles.[30,31]

Regarding the WVP, a significant increase was observed in all cases. In the case of spherical nanoparticles, at 20 wt% the WVP increases up to *ca* 200% and *ca* 100% for SNS20 and SNS100, respectively, and for SNL a large increase was observed reaching 115% at 10 wt%. The WVP increase caused by nanosphere loading was found to be inversely proportional to the particle diameter, suggesting that the water vapor is being adsorbed on the surface of the silica nanospheres due to the hydroxyl functional groups on the inorganic surface, which may interact with polar gases such as H_2O.[6,18] This behavior has previously been observed in PP/SiO_2 composites prepared using different diameters of silica nanospheres.[18,21] Furthermore, void formation and channels between adjacent particles in systems with poor dispersion, as discussed above, further increase the permeability. In the case of SNL, due to their high aspect ratio, preferential permeation channel formation further facilitates diffusion compared to the nanospheres. These results are consistent with the oxygen permeability results.[17] Moreover, it is also possible to see a significant increase of the WVP at low loadings; however, these increases are less pronounced compared to oxygen permeability. This is most probably due to the presence of a high organic content in the SNL (63.6%, from Table 1); thus the water vapor solubility is not increased as much as the oxygen solubility for a higher particle content. The M-F model results for WVP are smaller than the experimental results obtained in both cases (spherical and layered nanoparticles) because this model does not consider the solubility effect, which is more relevant in this case.

Mechanical properties

The elastic modulus of the PP/SiO_2 composites is illustrated in Fig. 5. When SNS20 or SNS100 are added, Young's modulus is increased (Fig. 5). The SNS20 have a stronger effect due to their higher specific surface area, increasing the stress transfer surface.[21] To understand these behaviors, the results obtained were compared to the Halpin–Tsai (H-T) model, which estimates the composite modulus using[32]

$$\frac{E_C}{E_m} = \frac{1 + 2\alpha\eta\phi}{1 - \eta\phi} \tag{5}$$

$$\eta = \frac{E_p/E_m - 1}{E_p/E_m + 2\alpha} \tag{6}$$

where ϕ is the particle volume fraction, α is the aspect ratio, E_p and E_m are the longitudinal stiffness for the particle and matrix, respectively, and E_c is the composite longitudinal elastic modulus. For composites with silica nanoparticles, these equations can be applied by assuming a particle stiffness E_p of 400 GPa.[14] The longitudinal stiffness of the matrix is $E_m = 951$ MPa (obtained experimentally). The aspect ratio of the SNS is 1 (spherical nanoparticles).[14] The H-T model for SNS20 underestimates the elastic modulus of the composite, as shown in Fig. 5. This model should estimate higher values since it assumes perfect adhesion between the particles and polymer, which is not chemically possible even in the presence of compatibilizers. An alternative to explain these higher experimental values is entanglement of the polymer chains with the SNS20, allowing load transfer and increasing the stiffness of the chains that surround the particles. To confirm this, the average diameter of the polymer is estimated by[33]

$$S^2 = aM^b \tag{7}$$

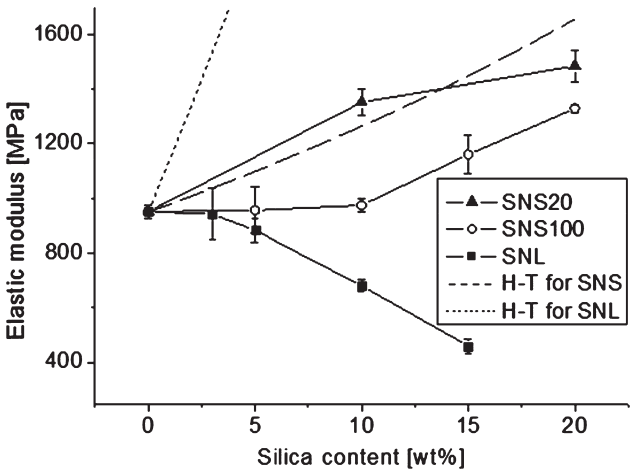

Figure 5. Elastic modulus of the prepared PP/SiO_2 composites.

$$d = \sqrt[2]{2S^2} \tag{8}$$

where S^2 is the mean square radius of gyration, M the molecular weight of the polymer, a and b are specific constants for each polymer, where for PP they take the values 0.1156 and 1.0, respectively,[33] and d is the average diameter of the polymer. The value obtained for the average diameter ($M \approx 290$ kg mol^{-1}) is *ca* 57 nm. The PP average diameter is larger than the average diameter of SNS20, and as a result entanglement of the polymer chains may occur, allowing load transfer and increasing the stiffness of the chains that surround the particles,[2,14] as has been previously reported for PP/SiO_2 composites.[14] For the SNS100 particles no significant effect was observed at loadings of 5 – 10 wt%.Only at higher loadings,15 and 20 wt%, was there a significant increase of 22% and 40%, respectively. In this case, as the diameter of the SNS100 is greater than the PP average diameter, entanglement of the polymer chains around these nanospheres is less likely to occur. Moreover, the results obtained experimentally are lower than the H-T model prediction, and thus the increase in stiffness is probably caused by the traditional load transfer mechanism (adhesion mechanism).

In the case of SNL, modification of some parameters is needed to account for their complex morphology in the H-T model:[14]

$$\alpha = \frac{L}{(N-1)\,d_{001} + d_s} \tag{9}$$

$$E_p = \frac{N}{t} E_s d_s \tag{10}$$

where L is the lateral size of the clay (*ca* 200 nm from Fig. 3(c)), t is the particle thickness(*ca* 1 nm[14]), E_s is the silica stiffness (400 GPa,[14] mentioned above), d_s and d_{001} are the thickness of individual clay sheets (*ca* 1 nm[11,14]) and the interlayer distance (4.8 nm as measured by XRD, Fig. 2) and N is the number of layers per stack and is assumed to be equal for all samples for simplicity (*ca* 15 units measured roughly in Fig. 3). In this case, the H-T model predicts composites with a dramatic increase in the elastic modulus with values as high as 1650 MPa at 5 wt% of SNL, whereas the experimental value was *ca* 883 MPa. These results can be explained by the appearance of interface defects produced during the blending process arising from internal stresses due to the mismatch between the particle and matrix thermal expansion

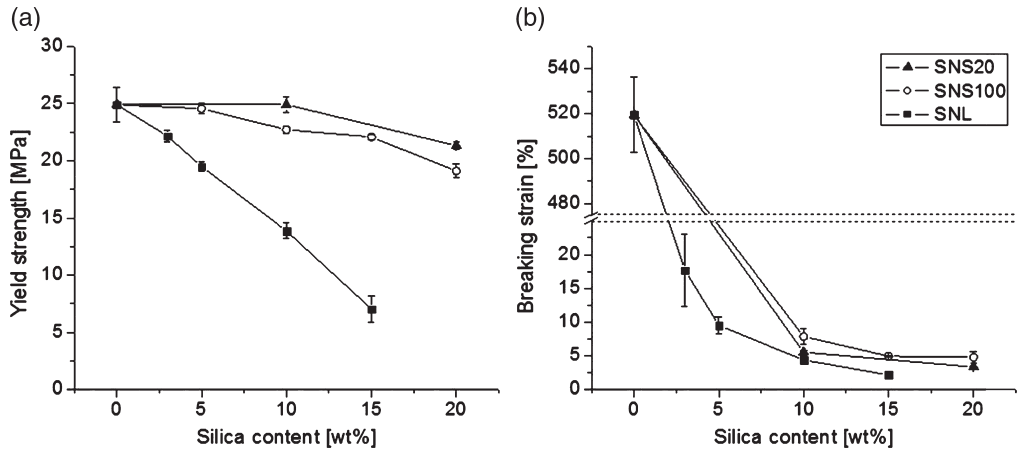

Figure 6. (a) Yield strength and (b) breaking strain of the prepared PP/SiO_2 composites.

coefficients, and in some cases gaseous products might also be formed at the interface.[34] Silica particles have a low thermal expansion coefficient (inorganic material) compared to polymers. When silica particles are dispersed in the polymer melt, the polymer chains contract upon cooling and will generate residual thermal stresses in the interface region. These residual stresses can generate small cracks under tensile loads, where part of the mechanical energy is used in the formation of the cracks.[6,34] Moreover, the TGA of the SNL particles showed that the degradation of the alkyl chains (C_{16}) begins at *ca* 180 °C, a temperature lower than the blending process temperature (190 °C); therefore, gases coming from this degradation would also generate cracks. In the literature, a decrease in the elastic modulus has been reported by Altan and Yildirim[35] in similar composites (PP/TiO_2) due to a poor particle – polymer interaction and agglomerate formation. Ash *et al.*[36] have also reported a decrease in elastic modulus in poly(methyl methacrylate)/alumina composites produced by the formation of voids within the polymer matrix and nanoparticle agglomerates that can act as crack initiators, leading to premature brittle failure. These voids are present in these composites, as discussed above, since the permeability to oxygen and water vapor mainly increased owing to their presence, especially in the case of the SNL (Fig. 4). Moreover, the TEM images (Fig. 3(c)) showed the presence of agglomerates, as mentioned above. It is noted that the particles cannot act as plasticizers because, although the elastic modulus decreases, the elongation at break also decreases (Fig. 6(b)).[37] Therefore the formation of voids, agglomerations and cracks in the polymer matrix is possibly responsible for the decrease in the elastic modulus in the PP/SNL composites.

Fig. 6 also shows the yield strength (Fig. 6(a)) and breaking strain (Fig. 6(b)) of the PP/SiO_2 composites. In general, the yield strength was reduced, reaching values of 14.5% and 23.7% at 20 wt% of SNS20 and SNS100, respectively, and a pronounced decrease of 71.9% at 15 wt% of SNL. On the other hand, the elongation at break decreases dramatically to over 99% with only 5 wt% in all cases. The decrease in yield strength occurs because in composites with poor particle – polymer interaction and agglomerations (previously mentioned) the material becomes brittle, since the applied stress cannot be effectively transmitted to the filler and the energy is fully absorbed by the polymer matrix.[6,13,38] The marked decrease in the breaking strain in these composites is due to the fact that silica nanoparticles are much stiffer than the PP; in fact the filling materials have virtually no deformation due to its high stiffness.[14] In addition, these nanoparticles strongly restrict the polymer chain movement when under stress, thus preventing the polymer chains from being extended and thereby reducing the plasticity of the material. This effect increases when there is no good polymer – particle interaction, which is what happens in these composites due to the agglomerations (Fig. 3), as discussed above.[6,13,38] The SNL nanoparticles have a greater effect than the spherical nanoparticles, possibly due to the lower surface area (Table 1), reducing even more the interaction area of the material. Similar results have been shown in PP with spherical silica nanoparticles and PP/clay composites.[6,21]

Thermal properties

Table 2 shows a summary of the TGA results for the PP/SiO_2 composites under inert conditions (N_2), and in all the cases an increase is seen in the onset of degradation temperature (T_{onset}) and in the maximum degradation temperature (T_{peak}), leading to an increase of up to 14.1, 3.8 and 6.4 °C in T_{onset} with 10 wt% of SNS20, SNS100 and SNL, respectively. The PP/SNS20 composites have the greatest effect on the thermal stability, increasing T_{onset} and T_{peak} by *ca* 10 °C compared to the other PP composites prepared at 10 wt%. Similar results have been found previously in PP/SiO_2 composites, where the nanoparticles improved the thermal behavior.[2,14]

According to the results of Table 2, the final residue (at 700 °C) of the nanocomposites approximately matches the mass fraction of incorporated nanoparticles. This indicates that incorporation of the nanoparticles does not promote coke formation in polymer degradation; therefore the improvements in thermal stability obtained cannot be explained by the mechanism of formation of a coke layer.[2,38] Regarding the stabilization based on the higher tortuosity rendered by the nanoparticles hindering the diffusion of volatile compounds ('labyrinth effect'), the presence of silica nanoparticles increases the oxygen permeability and WVP of the material (Fig. 4); consequently there is no evidence supporting this approach. Moreover, the radical stabilization mechanism due to the presence of metal ions, as reported for natural clays, is not applicable in this case, as the silica nanoparticles synthesized via sol-gel do not have metal ions.[2,12] On the other hand, it was found that the average diameter of this polymer (Eqn (8)) was *ca* 57 nm. From Figure 2, it can be confirmed that the interparticle distances are larger, at least two times for SNS20 and the SNL and four times for SNS100, than the diameter of the polymer chains. Therefore, the nano confinement effect does not occur. Moreover, because of the low polarity of the PP chains, chemical

Table 2. Effect of the nanoparticle size and charge on the onset temperature and degradation peak temperature (20 °C min^{-1}, N_2 atmosphere)

	SNS20			SNS100			SNL		
Load (wt%)	T_{onset} (°C)	T_{peak}(°C)	Residue (%)	T_{onset} (°C)	T_{peak} (°C)	Residue (%)	T_{onset} (°C)	T_{peak} (°C)	Residue (%)
0	425.0	460.0	2.5	425.0	460.0	2.5	425.0	460.0	2.5
5	430.7	464.6	6.8	426.2	461.5	6.4	426.7	463.5	6.9
10	439.1	472.6	9.5	428.8	463.2	9.1	431.4	465.5	10.5

interactions between the matrix and the nanoparticles can also be rejected, as in the case of spherical nanoparticles.[2,14] Therefore, the only plausible model explaining these experimental findings for PP/SiO_2 composites is the chemistry or physical adsorption of volatile compounds on the surface of these nanoparticles. When adsorbed, the volatile species are retained for a longer time preventing and/or lowering their diffusion-out, affecting the termination reactions promoted by recombination of radicals.[2,39] This model also explains why the SNS20 particles give the greatest stability to the polymer composite due to the larger surface area available for adsorption of the volatile molecules (Table 1).

CONCLUSIONS

The results with PP composites based on silica nanoparticles with different sizes and geometries provide relevant conclusions towards a better understanding of polymer nanocomposites. Silica nanospheres of 20 nm (SNS20) and 100 nm (SNS100) diameter and silica nanolayers (SNL) were successfully synthesized by the sol-gel method and blended with PP in the melt state to produce PP/SiO_2 nanocomposites. With regard to barrier properties, the oxygen and water vapor permeability increased, showing greater increase with SNL than with SNS probably due to a percolation effect. These increases are explained by the agglomeration of the nanoparticles due to the repulsive interaction of the hydrophilic silica surface and the hydrophobic PP matrix, interconnecting voids (free volume) that can partially or fully traverse the membrane. Regarding the mechanical behavior, SNS20 fillers increase the stiffness, showing that the mechanism for the mechanical reinforcement probably involves entanglements of polymer chains surrounding the nanoparticles, and for SNS100 the increase in stiffness is due to standard load transfer by the adhesion mechanism. In the case of SNL, the formation of voids, agglomerations and the degradation of the alkyl chains (C_{16}) present in the SNL in the blending process can produce small cracks in the composites, decreasing the elastic modulus. The thermal stability under inert conditions was improved in all cases, where the adsorption of volatile compounds on the surface of these nanoparticles can be responsible for these improvements.

ACKNOWLEDGEMENTS

The authors acknowledge with thanks the financial support under FONDECYT Project 1130446.

REFERENCES

1 Abraham R, Thomas SP, Kuryan S, Isac J, Varughese KT and Thomas S, *eXPRESS Polym Lett* **3**:177–189 (2009).
2 Palza H, Vergara R and Zapata P, *Macromol Mater Eng* **295**:899–905 (2010).
3 Choudalakis G and Gotsis AD, *Eur Polym J* **45**:967–984 (2009).
4 Rhim J-W, Park H-M and Ha C-S, *Prog Polym Sci* **38**:1629–1652 (2013).
5 Palza H, Gutiérrez S, Delgado K, Salazar O, Fuenzalida V, Avila JI *et al.*, *Macromol Rapid Commun* **31**:563–567 (2010).
6 Zou H, Wu S and Shen J, *Chem Rev* **108**:3893–3957 (2008).
7 Robertson GL, Packaging and food and beverage shelf life, in *Food and Beverage Stability and Shelf Life*, ed. by Kilcast D and Subramaniam P. Woodhead Publishing, Cambridge, UK, pp. 244–272 (2011).
8 Arora A and Padua GW, *J Food Sci* **75**:R43–R49 (2011).
9 Giannelis EP, *Adv Mater* **8**:29–35 (1996).
10 Alexandre M and Dubois P, *Mater Sci Eng R Rep* **28**:1–63 (2000).
11 Chastek TT, Que EL, Shore JS, Lowy R, Macosko C and Stein A, *Polymer* **46**:4421–4430 (2005).
12 Brinker CJ and Scherer GW, *Sol Gel Science: The Physics and Chemistry of Sol-Gel Processing*. Academic Press, San Diego, CA (1990).
13 Chen Y, Zhou S, Chen G and Wu L, *Prog Org Coatings* **54**:120–126 (2005).
14 Palza H, Vergara R and Zapata P, *Compos Sci Technol* **71**:535–540 (2011).
15 Jacquelot E, Espuche E, Gérard J-F, Duchet J and Mazabraud P, *J Polym Sci B Polym Phys* **44**:431–440 (2006).
16 Merkel TC, Freeman BD, Spontak RJ, He Z, Pinnau I, Meakin P *et al.*, *Sci* **296**:519–522 (2002).
17 Choudalakis G and Gotsis AD, *Curr Opin Colloid Interface Sci* **17**:132–140 (2012).
18 Dougnac VN, Alamillo R, Peoples BC and Quijada R, *Polymer* **51**:2918–2926 (2010).
19 Sinha Ray S and Okamoto M, *Prog Polym Sci* **28**:1539–1641 (2003).
20 Suprakas S, Kazunobu Y, Masami O, Akinobu O and Kazue U, *Chem Mater* **15**:1456–1465 (2003).
21 Bracho D, Dougnac V, Palza H and Quijada R, *J Nanomat* **2012**:Article ID 263915, 8 pp. (2012).
22 Moncada E, Quijada R and Retuert J, *Nanotechnology* **18**:Article ID 335606, 7 pp. (2007).
23 ASTM, *ASTM D 638-00: Standard Test Method for Tensile Properties of Plastics* (2000).
24 O'Brien KC, Koros WJ, Barbari TA and Sanders ES, *J Membr Sci* **29**:229–238 (1986).
25 Saito R and Hosoya T, *Polymer* **49**:4546–4551 (2008).
26 Hench LL and West JK, *Chem Rev* **90**:33–72 (1990).
27 Yoon PJ, Hunter DL and Paul DR, *Polymer* **44**:5323–5339 (2003).
28 Rozanski A, Monasse B, Szkudlarek E, Pawlak A, Piorkowska E, Galeski A *et al.*, *Eur Polym J* **45**:88–101 (2009).
29 Hashemifard SA, Ismail AF and Matsuura T, *J Membr Sci* **347**:53–61 (2010).
30 Garzón C and Palza H, *Compos Sci Technol* **99**:117–123 (2014).
31 Palza H, *eXPRESS Polym Lett* **6**:639–646 (2012).
32 Sheng N, Boyce MC, Parks DM, Rutledge GC, Abes JI and Cohen RE, *Polymer* **45**:487–506 (2004).
33 Zhou Z and Yan D, *Macromol Theory Simul* **6**:597–611 (1997).
34 Han Z and Fina A, *Prog Polym Sci* **36**:914–944.
35 Altan M and Yildirim H, *J Mater Sci Technol* **28**:686–692 (2012).
36 Ash BJ, Rogers DF, Wiegand CJ, Schadler LS, Siegel RW, Benicewicz BC *et al.*, *Polym Compos* **23**:1014–1025 (2002).
37 Jiang X, Jiang T, Gan L, Zhang X, Dai H and Zhang X, *Carbohydr Polym* **90**:1677–1684 (2012).
38 Leszczyńska A, Njuguna J, Pielichowski K and Banerjee JR, *Thermochim Acta* **453**:75–96 (2007).
39 Singh B and Sharma N, *Polym Degrad Stab* **93**:561–584 (2008).

